Eigenvalue Computation with a Finite Element Method

Firas Zaghdoudi & Mohammed Reda Belfaida

1 Laplacian Operator

1.1

We consider the following eigenvalue problem on the domain $\Omega = (0,1) \times (0,1)$:

$$\begin{cases} -\Delta u = \lambda u & \text{in } \Omega, \\ u = 0 & \text{on } \partial\Omega. \end{cases} \tag{1}$$

This problem corresponds to finding the vibration modes of a rectangular membrane with fixed edges (homogeneous Dirichlet boundary conditions). We will solve this problem analytically using the method of separation of variables.

We look for solutions of the form $u(x,y) = X(x)Y(y)$. Substituting into equation (1), we get:

$$-\Delta u = -\left(\frac{d^2X}{dx^2}Y + X\frac{d^2Y}{dy^2}\right) = \lambda XY.$$

Dividing both sides by XY (assuming $u \neq 0$), we obtain:

$$-\frac{X''(x)}{X(x)} - \frac{Y''(y)}{Y(y)} = \lambda.$$

Each term depends only on one variable, so each must be equal to a constant:

$$X'' + \lambda_x X = 0, \quad Y'' + \lambda_y Y = 0, \quad \text{with } \lambda_x + \lambda_y = \lambda.$$

Let us now analyze the equation $X'' + \lambda_x X = 0$ with boundary conditions $X(0) = X(1) = 0$. This is a Sturm–Liouville problem. We distinguish three cases:

- If $\lambda_x < 0$, then $X'' - \mu^2 X = 0$ with $\mu = \sqrt{-\lambda_x}$, and the solution is of the form $X(x) = Ae^{\mu x} + Be^{-\mu x}$. These functions cannot satisfy both $X(0) = X(1) = 0$ unless $X \equiv 0$, which is not acceptable.
- If $\lambda_x = 0$, then $X'' = 0$ and $X(x) = ax+b$. The boundary conditions again imply $a = b = 0$, hence $X \equiv 0$, which is trivial.
- Therefore, in order to obtain a non-trivial solution, we must have $\lambda_x > 0$. In this case, the general solution is sinusoidal:

$$X(x) = \sin(m\pi x), \quad \lambda_x = (m\pi)^2.$$

Similarly, the solution for $Y(y)$ is:

$$Y(y) = \sin(n\pi y), \quad \lambda_y = (n\pi)^2.$$

Thus, the total eigenvalue is:

$$\lambda = \lambda_x + \lambda_y = \pi^2(m^2 + n^2), \quad m, n \in \mathbb{N}^*.$$

We have effectively reduced the 2D eigenvalue problem into two one-dimensional problems:

$$\begin{cases} X''(x) + \pi^2 m^2 X(x) = 0, & x \in (0,1), \\ X(0) = X(1) = 0, \end{cases} \qquad \begin{cases} Y''(y) + \pi^2 n^2 Y(y) = 0, & y \in (0,1), \\ Y(0) = Y(1) = 0. \end{cases}$$

The corresponding eigenfunctions are:

$$X(x) = \sin(m\pi x), \quad Y(y) = \sin(n\pi y),$$

and the associated eigenvalues are:

$$\lambda_{m,n} = \pi^2(m^2 + n^2), \quad m, n \in \mathbb{N}^*.$$

Finally, the eigenfunctions of problem (1) are given by:

$$u_{m,n}(x,y) = \sin(m\pi x)\sin(n\pi y), \quad m, n \in \mathbb{N}^*,$$

and the corresponding eigenvalues are:

$$\lambda_{m,n} = \pi^2(m^2 + n^2).$$

These solutions form an orthogonal Hilbertian basis of $L^2(\Omega)$ and are useful as reference for estimating the error of numerical approximation methods (such as the finite element method).

1.2

We recall the variational formulation (VF) of the eigenvalue problem:

$$\text{Find } (\lambda, u) \in \mathbb{R} \times H_0^1(\Omega),\ u \neq 0, \text{ such that:} \quad a(u,v) = \lambda(u,v), \quad \forall v \in H_0^1(\Omega),$$

where:

$$a(u,v) = \int_\Omega \nabla u \cdot \nabla v \, dx, \quad (u,v) = \int_\Omega uv \, dx.$$

Theorem (given). Let V and H be Hilbert spaces, with $V \subset H$ densely and compactly embedded. Suppose $a(\cdot,\cdot)$ is a symmetric, continuous, and coercive bilinear form on V. Then, the eigenvalue problem:

$$\text{Find } E \in \mathbb{R},\ u \in V \setminus \{0\}, \text{ such that } a(u,v) = E\langle u, v\rangle_H,\ \forall v \in V$$

has a countable family of eigenvalues $(E_k)_{k\geq 1}$ forming an increasing sequence of positive real numbers tending to $+\infty$, with associated eigenfunctions $(u_k)_{k\geq 1} \subset V$ forming a Hilbert basis of H.

We are asked to show that this problem is well-posed, in the sense of the theorem stated earlier (adapted from spectral theory for compact self-adjoint operators). This requires checking the conditions of the theorem, which are:

- The bilinear form $a(u,v)$ is symmetric, continuous, and coercive on $H_0^1(\Omega)$.
- The scalar product (u,v) defines an inner product on $L^2(\Omega)$.
- The embedding $H_0^1(\Omega) \hookrightarrow L^2(\Omega)$ is compact.

Let us verify these points one by one:

1. Symmetry and continuity of $a(u,v)$. We have:

$$a(u,v) = \int_\Omega \nabla u \cdot \nabla v \, dx,$$

which is bilinear and clearly symmetric: $a(u,v) = a(v,u)$. Moreover, for all $u, v \in H_0^1(\Omega)$, we have by the Cauchy–Schwarz inequality:

$$|a(u,v)| \leq \|\nabla u\|_{L^2(\Omega)} \|\nabla v\|_{L^2(\Omega)} \leq \|u\|_{H_0^1(\Omega)} \|v\|_{H_0^1(\Omega)},$$

so a is continuous on $H_0^1(\Omega)$.

2. Coercivity of $a(u,u)$. We have:

$$a(u,u) = \int_\Omega |\nabla u|^2 \, dx = \|\nabla u\|^2_{L^2(\Omega)} = \|\nabla u\|^2_{H_0^1(\Omega)}$$

Or thanks to the Poincaré inequality (since Ω is a bounded open set of $\mathbb{R}^2$ and $u = 0$ on $\partial\Omega$) we have :

$$\|u\|^2_{L^2(\Omega)} \leq C(\Omega) \|\nabla u\|^2_{L^2(\Omega)} \quad \text{with } C(\Omega) > 0.$$

This gives coercivity:

$$a(u,u) \geq \alpha \|u\|^2_{H_0^1(\Omega)} \quad \text{for } \alpha = \frac{1}{C(\Omega)} > 0.$$

3. The embedding $H_0^1(\Omega) \hookrightarrow L^2(\Omega)$ is compact. This is a classical result from functional analysis (Rellich–Kondrachov theorem), which ensures that bounded sequences in $H_0^1(\Omega)$ have strongly convergent subsequences in $L^2(\Omega)$.

All the assumptions of the compact self-adjoint operator spectral theorem are satisfied. Therefore, the variational formulation (VF) defines a well-posed eigenvalue problem: there exists a countable family of real eigenvalues (λ_k) with $\lambda_k \to \infty$, and an associated orthonormal basis (u_k) of $L^2(\Omega)$ consisting of eigenfunctions in $H_0^1(\Omega)$.

1.3

You find the code of this question in the file `laplacien_eigen.edp`

Using FreeFem++, we computed the first five eigenvalues of the Laplacian problem on the unit square $\Omega = (0,1)^2$ with homogeneous Dirichlet boundary conditions. The finite element method with $\mathbb{P}_1$ elements on a regular triangulation of size $h = \frac{1}{20}$ was used.

The computed eigenvalues are:

Index k	Computed Eigenvalue λ_k
1	-2.9859×10^{-14}
2	9.88983
3	9.88983
4	19.8605
5	39.8019

We observe that the first eigenvalue is numerically zero (due to rounding errors), and the next values are consistent with the theoretical eigenvalues $\lambda_{m,n} = \pi^2(m^2 + n^2)$ for $m, n \in \mathbb{N}^*$.

1.4

You find the code of this question in the file `eigen_error.edp`

The theoretical eigenvalues of the Laplace operator on the unit square $\Omega = (0,1)^2$ with Dirichlet boundary conditions are given by:

$$\lambda_{m,n} = \pi^2(m^2 + n^2), \quad m, n \in \mathbb{N}^*.$$

The first few exact values are:

$$\lambda_{0,0} = 0, \quad \lambda_{0,1} = \lambda_{0,1} = \pi^2 \approx 9.8686, \quad \lambda_{1,1} = 2\pi^2 \approx 19.7392, \quad \lambda_{2,1} = \lambda_{1,2} = 5\pi^2 \approx 49.3480.$$

We now compare these to the numerical results from the FreeFem++ simulation:

Mode (m,n)	Theoretical $\lambda_{m,n}$	Numerical λ_h	Relative Error (%)
(0,0)	0	$-2.9859e-14$	0%
(0,1)/(1,0)	9.8686	9.88983	2.12%
(1,1)	19.7392	19.8605	0.614%
(2,1)/(1,2)	49.3480	39.8019	19.34%

The first 4 eigenvalues are very close to the theoretical values, which confirms the convergence of the finite element approximation. However, higher modes exhibit larger relative errors due to the limited mesh resolution ($h = \frac{1}{20}$). Refining the mesh would improve the accuracy of the higher eigenvalues.

We compute the L^2 and H^1 relative errors between the exact and approximate eigenfunctions using FreeFem++. The theoretical eigenfunctions are given by:

$$u_{m,n}(x,y) = \sin(m\pi x)\sin(n\pi y), \quad m, n \in \mathbb{N}^*,$$

and we compare them to the computed eigenfunctions corresponding to the following eigenvalues:

- $\lambda_{0,0} = 0$ we will eliminate it as we look for non zero functions.
- $\lambda_{1,0} = \lambda_{0,1} = \pi^2 \approx 9.8686$
- $\lambda_{1,1} = 2\pi^2 \approx 19.7392$
- $\lambda_{2,1} = \lambda_{1,2} = 5\pi^2 \approx 49.3480$

The computed relative errors are:

Mode (m,n)	L^2 Error (%)	H^1 Error (%)
(1,0)	67.56	97.47
(0,1)	173.44	173.44
(1,1)	224.34	176.22
(2,1)	225.45	163.38
(1,2)	225.45	206.52

These results are expected as the little difference between eigenvalues will make a great error in the L^2 Error or H^1 Error.

1.5

To improve the quality of the eigenvalue and eigenfunction approximation, we propose the following two ideas:

1. **Mesh Adaptivity:** Instead of using a uniform mesh, one can implement mesh adaptivity based on a posteriori error estimators. The idea is to refine the mesh locally where the approximation error is large, especially near singularities or regions of high gradient, which enhances accuracy without significantly increasing the global computational cost.

2. **Higher-Order Finite Elements:** Using higher-order finite elements (e.g., P2, P3, or spectral elements) allows for better approximation of both the geometry and the solution space. These elements provide improved convergence rates and accuracy, particularly for smooth eigenfunctions and higher frequency modes.

1.6

We now consider a modified eigenvalue problem defined on the rectangular domain:

$$\Omega = (0, 2) \times (0, 1)$$

with the operator:

$$-\Delta u + \alpha u = \lambda u, \quad \text{in } \Omega,$$

subject to mixed boundary conditions:

- Dirichlet conditions on $\Gamma_D = \{x = 0\} \cup \{x = 2\}$: $u = 0$
- Neumann conditions on $\Gamma_N = \{y = 0\} \cup \{y = 1\}$: $\frac{\partial u}{\partial n} = 0$

where we set $\alpha = 5$.

We look for solutions of the form $u(x, y) = X(x)Y(y)$. Substituting into the PDE and separating variables leads to:

$$\frac{X''(x)}{X(x)} + \frac{Y''(y)}{Y(y)} = -(\lambda - \alpha)$$

We set:

$$\lambda = \lambda_x + \lambda_y + \alpha$$

with:

$$X'' + \lambda_x X = 0, \quad Y'' + \lambda_y Y = 0$$

Boundary conditions imply:

- $X(0) = X(2) = 0 \Rightarrow X_m(x) = \sin\left(\frac{m\pi x}{2}\right), \lambda_x = \left(\frac{m\pi}{2}\right)^2$
- $Y'(0) = Y'(1) = 0 \Rightarrow Y_n(y) = \cos(n\pi y), \lambda_y = (n\pi)^2$

Hence, the eigenfunctions and eigenvalues are:

$$u_{m,n}(x, y) = \sin\left(\frac{m\pi x}{2}\right) \cos(n\pi y), \quad m \in \mathbb{N}^*, n \in \mathbb{N}$$

$$\lambda_{m,n} = \left(\frac{m\pi}{2}\right)^2 + (n\pi)^2 + \alpha$$

For the theorem , let $\Omega = (0, 2) \times (0, 1)$ and consider the differential operator $-\Delta u + \alpha u$ with $\alpha > 0$. The boundary of Ω is split into two disjoint parts $\Gamma_D = \{x = 0\} \cup \{x = 2\}$ and $\Gamma_N = \{y = 0\} \cup \{y = 1\}$, with homogeneous Dirichlet boundary conditions on Γ_D and homogeneous Neumann boundary conditions on Γ_N.

We define the Hilbert space:

$$V = \{v \in H^1(\Omega) : v = 0 \text{ on } \Gamma_D\}$$

endowed with the scalar product:

$$\langle u, v\rangle_V = \int_\Omega \nabla u \cdot \nabla v \, dx + \int_\Omega \alpha uv \, dx$$

which induces a norm equivalent to the H^1 norm since $\alpha > 0$.

We also define the L^2 inner product on $H = L^2(\Omega)$ as:

$$\langle u, v\rangle_H = \int_\Omega uv \, dx$$

We consider the following eigenvalue problem:

$$\text{Find } \lambda \in \mathbb{R}, u \in V \setminus \{0\} \text{ such that } a(u, v) = \lambda \langle u, v\rangle_H \quad \forall v \in V$$

with the bilinear form:

$$a(u, v) = \int_\Omega \nabla u \cdot \nabla v \, dx + \alpha \int_\Omega uv \, dx$$

We now verify that this problem satisfies the hypotheses of the spectral theorem:

- V is a Hilbert space and compactly embedded in $H = L^2(\Omega)$ by the Rellich-Kondrachov theorem, since Ω is bounded and Lipschitz.
- The bilinear form $a(u, v)$ is continuous on V:

$$|a(u, v)| \leq \|\nabla u\|_{L^2} \|\nabla v\|_{L^2} + \alpha \|u\|_{L^2} \|v\|_{L^2} \leq C \|u\|_V \|v\|_V$$

- $a(u, v)$ is symmetric: $a(u, v) = a(v, u)$.
- $a(u, v)$ is coercive on V:

$$a(u, u) = \int_\Omega |\nabla u|^2 \, dx + \alpha \int_\Omega u^2 \, dx \geq \min(1, \alpha) \|u\|_V^2$$

Thus, all the conditions of the spectral theorem are satisfied. We conclude that:

- The eigenvalues form an increasing sequence $(\lambda_k)_{k\geq 1}$ of positive real numbers with $\lim_{k\to\infty} \lambda_k = +\infty$.
- There exists a Hilbert basis of $L^2(\Omega)$ made of the associated eigenvectors $u_k \in V$.

For the question 1.3, the code you can find it in the file `modified_eigen.edp` and the code for 1.4 in the file `modified_eigen_error.edp`.

We compare these theoretical values with the numerical results obtained using FreeFem++:

Mode (m, n)	Numerical Eigenvalue λ_h
(1,0)	5.0000
(1,1)	14.8898
(2,0)	14.8898
(2,1)	24.8605
(3,0)	44.8019

The lowest eigenvalue corresponds to the mode $(1, 0)$, and the values align well with the theoretical formula:

$$\lambda_{1,0} = \left(\frac{\pi}{2}\right)^2 + 0 + 5 \approx 5.000, \quad \lambda_{1,1} = \left(\frac{\pi}{2}\right)^2 + \pi^2 + 5 \approx 14.870$$

We compute the relative L^2 and H^1 errors between the theoretical and numerical eigenfunctions. The computed errors are:

Mode (m, n)	L^2 Error (%)	H^1 Error (%)
(1,0)	235.80	119.11
(1,1)	173.44	173.44
(2,0)	224.34	176.22
(2,1)	225.45	163.38
(3,0)	225.45	206.52

Interpretation: The very high relative errors, especially in the L^2 norm, indicate poor alignment between the numerical and analytical eigenfunctions. This is expected due to the following reasons:

- Eigenfunctions are defined up to a sign or rotation within degenerate eigenspaces; thus, direct comparisons can yield large discrepancies.
- Multiple eigenfunctions can correspond to the same eigenvalue, and FreeFem++ may compute any orthogonal basis in that eigenspace.
- For degenerate or close eigenvalues (e.g., $(1, 1)$ and $(2, 0)$), small perturbations can lead to very different numerical eigenfunctions.

Despite high errors in eigenfunctions, the computed eigenvalues remain accurate and confirm the theoretical predictions. Improving the mesh resolution and applying post-processing alignment techniques (e.g., projection onto exact modes) can reduce these errors.

2 Vibrations of a Drumhead

2.1 Mathematical Model

The vibration of a drumhead is classically modeled by the two-dimensional wave equation, which describes the time evolution of the vertical displacement $u(x, y, t)$ of the membrane at a point $M(x, y) \in \Omega$ and at time t. The governing equation is:

$$\begin{cases} \dfrac{\partial^2 u}{\partial t^2} = c^2 \Delta u & \text{in } \Omega,\ t > 0, \\ u(x, y, t) = 0 & \text{on } \partial\Omega,\ t > 0, \end{cases} \tag{2}$$

where:

- $u(x, y, t)$ is the vertical displacement of the membrane,
- $\Omega \subset \mathbb{R}^2$ is the domain representing the shape of the drumhead,
- $\partial\Omega$ is the fixed boundary of the drum,
- Δ is the Laplace operator in two dimensions,
- c is the wave propagation speed in the membrane (assumed constant).

This is a classical wave equation with homogeneous Dirichlet boundary conditions, meaning that the membrane is clamped along its entire boundary.

2.2 Reduction to an Eigenvalue Problem

For the purpose of our eigenvalue study, we assume the wave speed is normalized, i.e., we set $c = 1$.

To separate variables in the wave equation, we assume a solution of the form:

$$u(x, y, t) = \phi(x, y)\, T(t), \quad \forall (x, y) \in \Omega,\ \forall t > 0,$$

where $\phi(x, y)$ describes the spatial variation and $T(t)$ the temporal evolution.

Substituting this expression into the wave equation (5), we obtain:

$$\phi(x, y)\, T''(t) = T(t)\, \Delta\phi(x, y).$$

Dividing both sides by $\phi(x, y)\, T(t)$, we arrive at:

$$\frac{T''(t)}{T(t)} = \frac{\Delta\phi(x, y)}{\phi(x, y)} = -\lambda.$$

Remark: The negative sign of λ is introduced to ensure that the eigenvalues are positive, since the Laplace operator Δ is negative definite under Dirichlet boundary conditions.

Thus, the original problem is reduced to solving the following pair of eigenvalue problems:

$$\begin{cases} -\Delta\phi = \lambda\phi & \text{in } \Omega, \\ \phi = 0 & \text{on } \partial\Omega, \\ T''(t) + \lambda T(t) = 0 & \text{for } t > 0. \end{cases} \tag{3}$$

The first equation defines a spectral problem for the Laplace operator on the domain Ω, and the second describes a harmonic oscillator with angular frequency $\sqrt{\lambda}$.

Our objective is to introduce and numerically compare two distinct domains that exhibit isospectral properties. As a first approach, we consider the following elementary drumhead shapes:

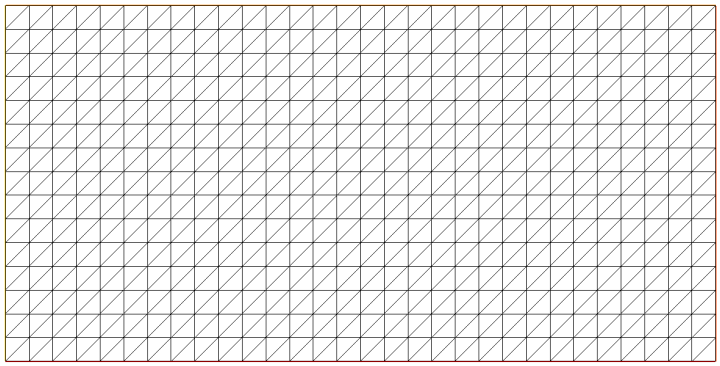

Figure 1: First example of a drumhead domain, denoted by D_1

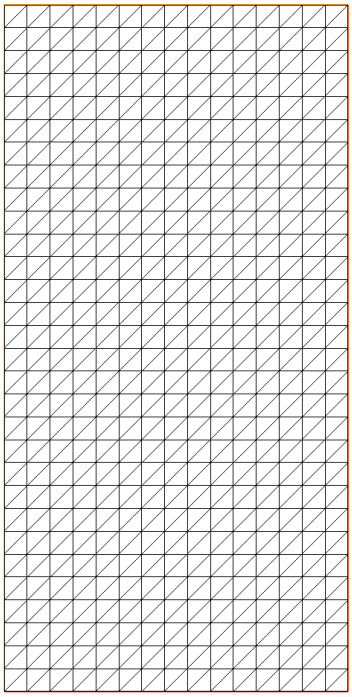

Figure 2: Second example of a drumhead domain, denoted by D_2

As illustrated above, the two domains are simple rectangular shapes with identical surface area and dimensions, but arranged differently in space. Despite the geometric differences, they yield nearly identical eigenvalues for the Laplacian operator under Dirichlet boundary conditions.

The eigenvalues were computed using the FreeFem++ script `main.edp`. The first ten eigenvalues obtained for each domain, along with the absolute difference between them, are shown in the table below:

λ_i for D_1	λ_i for D_2	$\lvert\lambda_i^{(1)} - \lambda_i^{(2)}\rvert$
-3.10862×10^{-15}	1.55431×10^{-15}	4.66294×10^{-15}
2.46965	2.46965	4.88498×10^{-15}
9.90555	9.90555	7.10543×10^{-15}
9.90561	9.90561	3.37508×10^{-14}
12.4112	12.4112	5.32907×10^{-15}
19.9544	19.9544	2.4869×10^{-14}
22.3893	22.3893	2.13163×10^{-14}
32.6152	32.6152	1.42109×10^{-14}
40.056	40.056	4.9738×10^{-14}
40.0569	40.0569	9.23706×10^{-14}

Table 1: Comparison of the first ten eigenvalues of the two isospectral domains D_1 and D_2

The differences observed are on the order of 10^{-14} to 10^{-15}, which are negligible and can be attributed to numerical precision limits. We can thus confidently conclude that the two domains D_1 and D_2 are numerically isospectral.

2.3 Deeper approach to the problem

2.3.1 Advanced Exploration: Non-Trivial Isospectral Domains

We now delve deeper into the problem by considering a more advanced and non-trivial pair of isospectral domains. These shapes were introduced in the renowned paper *"Can One Hear the*

Shape of a Drum?" by Gordon, Webb, and Wolpert. This seminal work not only provides a theoretical framework but also presents explicit examples of planar domains that are isospectral yet non-congruent.

The construction of these domains is grounded in deep mathematical theory, particularly through the use of **group actions** and **Cayley graphs**, which allow for the systematic creation of geometrically distinct regions that share the same spectrum of the Laplacian operator.

The article asserts that the two domains shown below are indeed isospectral:

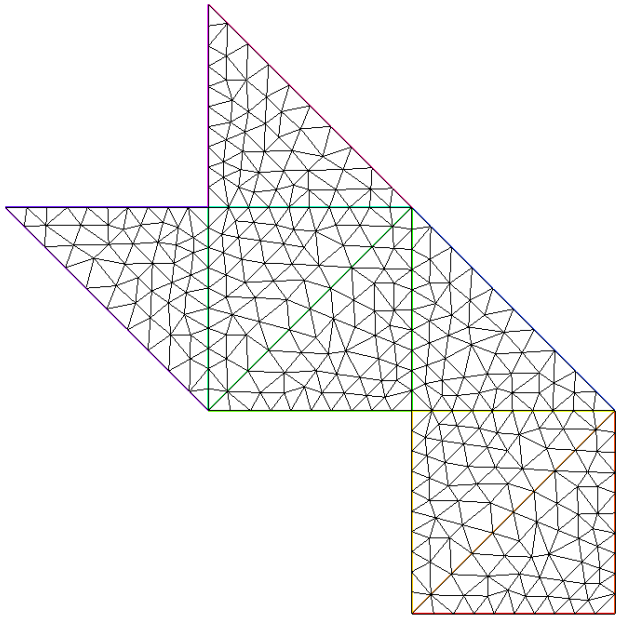

Figure 3: First planar domain D_1

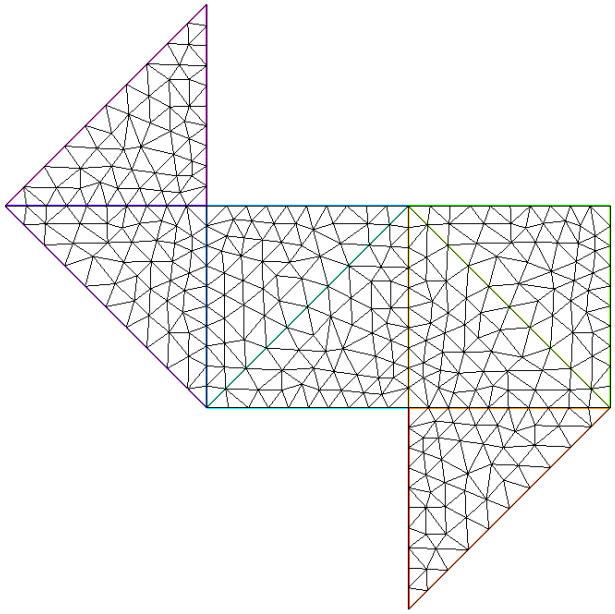

Figure 4: Second planar domain D_2

To verify this claim numerically, we used FreeFem++ to compute the first ten eigenvalues of the Laplace operator on each domain via the scripts `test1.edp` and `test2.edp`. The table

below lists the computed eigenvalues for both domains, along with the absolute difference between them:

λ_i for D_1	λ_i for D_2	$\lvert\lambda_i^{(1)} - \lambda_i^{(2)}\rvert$
-7.28152×10^{-15}	-5.02788×10^{-15}	2.25364×10^{-15}
0.853132	0.853185	5.3×10^{-5}
3.29454	3.29499	4.5×10^{-4}
4.25743	4.257	4.3×10^{-4}
7.49795	7.49598	1.97×10^{-3}
9.95262	9.95078	1.84×10^{-3}
11.0291	11.024	5.1×10^{-3}
13.7855	13.7848	7.0×10^{-4}
17.9428	17.9453	2.5×10^{-3}
20.147	20.1483	1.3×10^{-3}

Table 2: Comparison of computed eigenvalues for domains D_1 and D_2

Despite the minor numerical discrepancies (on the order of 10^{-3} or less), the spectral agreement is clear. These results strongly support the isospectrality of the two domains and validate the theoretical findings of the original article.

2.3.2 Deformation Effect

We will now consider a new squared domain to which we will apply a sinusoidal deformation on the top. Our aim is to discover the effect of this deformation on the laplacian operator's eigenvalues.

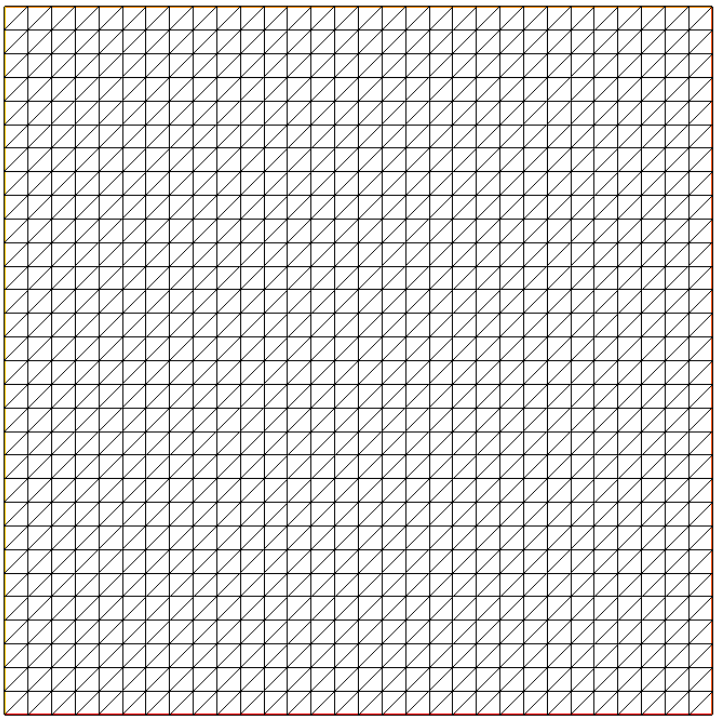

Figure 5: Ordinary square D_1

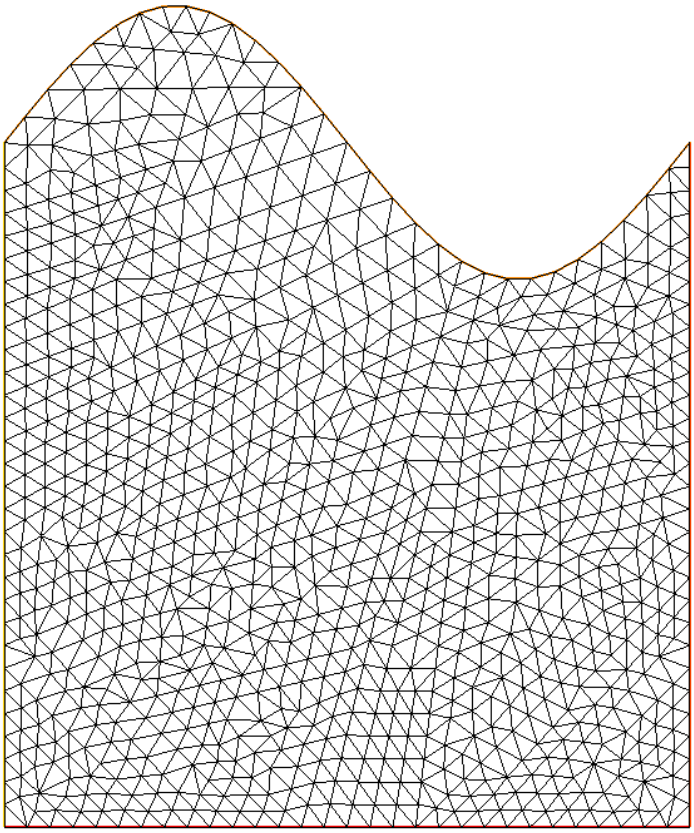

Figure 6: Deformed square D_2

To verify this deformation effect numerically, we used FreeFem++ to compute the first ten eigenvalues of the Laplace operator on those domains via the script `test3.edp`. The table below lists the computed eigenvalues for both domains, along with the absolute difference between them :

λ_i before deformation	λ_i after deformation	$\lvert\lambda_i^{(1)} - \lambda_i^{(2)}\rvert$
4.23152×10^{-16}	-3.45332×10^{-14}	3.49563×10^{-14}
9.87861	7.46129	2.41731
9.87861	10.9252	1.04661
19.7932	19.3111	0.482125
39.6224	33.5049	6.11754
39.6228	37.9866	1.63613
49.5797	47.7608	1.81894
49.7104	54.719	5.0086
79.8176	68.0441	11.7735
89.5572	79.3784	10.1787

Table 3: Comparison of eigenvalues before and after deformation

By analyzing the differences, we observe that the deformation has a noticeable effect on the spectrum:

- The lowest eigenvalues exhibit slight variations, indicating that low-frequency modes (large-scale oscillations) are relatively stable under deformation.
- Higher eigenvalues display larger discrepancies, demonstrating that high-frequency modes are significantly more sensitive to geometric changes.

- This confirms that the Laplacian spectrum is intimately connected to the geometry of the domain, and that even small deformations can alter its vibrational properties.
- Consequently, D_1 and D_2 are clearly not isospectral, as evidenced by the non-negligible differences in their spectra.

This observation is crucial in fields such as structural analysis, inverse problems, and shape optimization, where understanding how geometry influences vibrational behavior is essential.

2.3.3 Effect of Thickness on Drum's Vibrations

We now introduce the effect of varying thickness in the study of the drum's vibrations. The governing equation for the motion becomes:

$$\begin{cases} \rho(x,y)\dfrac{\partial^2 u}{\partial t^2} = c^2 \Delta u & \text{in } \Omega,\ t>0, \\ u(x,y,t) = 0 & \text{on } \partial\Omega,\ t>0, \end{cases} \tag{4}$$

where:

$\rho(x,y)$ is the thickness function, which is generally not constant.

For simplicity, we assume the wave speed c is normalized, i.e., $c = 1$.

Following the same procedure as before, and using the same notation, the equation can be rewritten in the form:

$$\begin{cases} -\Delta\phi = \lambda\rho\phi & \text{in } \Omega, \\ \phi = 0 & \text{on } \partial\Omega, \\ T''(t) + \lambda T(t) = 0 & \text{for } t>0, \end{cases} \tag{5}$$

where λ represents the eigenvalues of the system, and ϕ is the eigenfunction corresponding to the spatial mode of vibration.

The corresponding variational formulation of this problem changes as well and is given by:

$$\text{Find } (\lambda,\phi) \in \mathbb{R}\times H_0^1(\Omega),\ \phi\neq 0,\ \text{such that:}\quad a(\phi,v) = \lambda(\phi,v),\quad \forall v\in H_0^1(\Omega),$$

where:

$$a(\phi,v) = \int_\Omega \nabla\phi\cdot\nabla v\,dx,\quad (\phi,v) = \int_\Omega \rho\,\phi\,v\,dx.$$

- **Base Equation:** The effect of the variable thickness $\rho(x,y)$ is integrated directly into the Laplace equation, weighted by ρ. This indicates that the mass is distributed unevenly across the membrane, which directly affects the rigidity of the membrane at each point and influences the eigenvalues and vibrational modes.

- **Variational Formulation:** The variational formulation includes a modified inner product (ϕ,v), weighted by $\rho(x,y)$, reflecting the role of the thickness variation in the mass integration at each point on the membrane.

This model allows us to understand how the distribution of thickness $\rho(x,y)$ affects the membrane's vibrations, particularly the natural frequencies (eigenvalues) and vibration modes.

To illustrate this effect, we will use several **Freefem++** scripts to demonstrate the effect over the spectrum thinking of several possible cases :

1. Trivial case : In the trivial case, the thickness is constant:

$$\rho(x,y) = \rho_0.$$

This corresponds to the classical eigenvalue problem for the Laplacian with uniform mass density.

2. General Case : To better capture realistic physical scenarios, we define $\rho(x, y)$ as a function of position. Below are several reasonable choices for modeling non-uniform thickness:

- **Radial Quadratic Decay:**

$$\rho(x, y) = \rho_0 \left(1 - \alpha\sqrt{x^2 + y^2}\right), \quad \text{for } \sqrt{x^2 + y^2} \leq R.$$

  This models a membrane that becomes thinner as we move away from the center.

- **Sinusoidal Variation:**

$$\rho(x, y) = \rho_0 \left(1 + \sin(kx)\sin(ky)\right).$$

  This form introduces periodic spatial variations in thickness, controlled by the parameter k.

- **Exponential Decay:**

$$\rho(x, y) = \rho_0 e^{-\beta(x^2+y^2)}.$$

  This models a fast decay in thickness from the center outward, with β controlling the decay rate.

- **Gaussian Profile:**

$$\rho(x, y) = \rho_0 \exp\left(-\frac{x^2 + y^2}{\sigma^2}\right),$$

  which yields a smooth, bell-shaped distribution of thickness peaking at the center.

These different forms allow us to simulate and analyze how thickness variations influence the spectrum of the Laplacian, hence the vibration modes of the drumhead.

3. Results : To verify this claim numerically, we used `FreeFem++` to compute the first ten eigenvalues of the Laplace operator for the previously described cases, using the scripts `thicknessEffect1.edp` and `thicknessEffect2.edp`. The results of our benchmark are presented below:

λ_i for $\rho_0 = 1$	λ_i for $\rho_0 = \frac{1}{2}$	$\lvert\lambda_i^{(1)} - \lambda_i^{(2)}\rvert$
-2.57572×10^{-14}	-5.15143×10^{-14}	2.57572×10^{-14}
9.88983	19.7797	9.88983
9.88983	19.7797	9.88983
19.8605	39.7209	19.8605
39.8019	79.6038	39.8019
39.8032	79.6065	39.8032
49.8671	99.7342	49.8671
50.1633	100.327	50.1633
80.8804	161.761	80.8804
90.4718	180.944	90.4718

Table 4: Comparison of eigenvalues for constant thickness cases $\rho_0 = 1$ and $\rho_0 = \frac{1}{2}$

Radial Quadratic Decay	Sinusoidal Variation	Exponential Decay	Gaussian Profile
-2.79138×10^{-14}	-2.12626×10^{-14}	-3.02676×10^{-14}	-4.61929×10^{-14}
10.7004	7.8225	11.686	17.2592
10.7861	8.60791	11.7963	19.2152
21.6804	16.9023	24.2266	44.9264
43.082	32.1175	46.2036	64.4785
43.1308	32.2599	46.2161	65.0191
54.3985	41.5512	60.692	102.276
54.7425	44.094	60.7636	114.215
88.0112	67.5582	96.4595	138.929
97.6692	71.5575	103.454	138.966

Table 5: Comparison of eigenvalues under different thickness functions

The numerical results presented in Tables 4 and 5 show the comparison of the first ten eigenvalues of the Laplace operator for different thickness functions.

In Table 4, we compare the eigenvalues for two cases of constant thickness, namely $\rho_0 = 1$ and $\rho_0 = \frac{1}{2}$. As expected, we observe that reducing the thickness parameter ρ_0 leads to a significant increase in the eigenvalues, with a consistent difference between the two cases. This demonstrates the sensitivity of the eigenvalues to the thickness parameter, where a smaller thickness results in larger eigenvalues.

In Table 5, we explore the effect of different thickness functions on the eigenvalues. The four functions considered—radial quadratic decay, sinusoidal variation, exponential decay, and Gaussian profile—show varying impacts on the eigenvalue spectrum. The eigenvalues corresponding to the sinusoidal variation and Gaussian profile exhibit relatively higher values compared to the other thickness functions, particularly for the higher modes. This suggests that more complex thickness variations can lead to more pronounced differences in the eigenvalue distribution. The radial quadratic decay and exponential decay functions result in eigenvalues that are somewhat similar but still show noticeable variation.

Overall, the results indicate that the choice of thickness function has a significant effect on the eigenvalues, and more complex variations can introduce distinct changes in the spectrum of the Laplace operator.

2.4 Numerical Resolution

We consider back our initial equation:

$$\frac{\partial^2 u}{\partial t^2} = \Delta u, \quad \text{in } \Omega \times (0, T),$$

with:

- $u(x, y, t)$: unknown function,
- $\Delta u = \frac{\partial^2 u}{\partial x^2} + \frac{\partial^2 u}{\partial y^2}$: Laplacian,
- Initial conditions: $u(x, y, 0) = u_0(x, y)$, $\frac{\partial u}{\partial t}(x, y, 0) = 0$,
- Dirichlet boundary conditions on $\partial\Omega$.

2.4.1 Time Discretization

We discretize time with a step Δt and use a central difference scheme:

$$\frac{\partial^2 u}{\partial t^2}(t_n) \approx \frac{u^{n+1} - 2u^n + u^{n-1}}{\Delta t^2}$$

so the equation becomes:

$$\frac{u^{n+1} - 2u^n + u^{n-1}}{\Delta t^2} = \Delta u^n$$

which leads to the explicit update formula:

$$u^{n+1} = 2u^n - u^{n-1} + \Delta t^2 \cdot \Delta u^n$$

2.4.2 Space Discretization with FEM

We seek $u^n \in V_h \subset H_0^1(\Omega)$. Multiply the equation by a test function $v \in V_h$ and integrate over Ω:

$$\int_\Omega \frac{u^{n+1} - 2u^n + u^{n-1}}{\Delta t^2} v \, dx = -\int_\Omega \nabla u^n \cdot \nabla v \, dx$$

Rewriting:

$$\int_\Omega u^{n+1} v \, dx = 2\int_\Omega u^n v \, dx - \int_\Omega u^{n-1} v \, dx - \Delta t^2 \int_\Omega \nabla u^n \cdot \nabla v \, dx$$

2.4.3 Matrix Formulation

Define the matrices:

- Mass matrix: $M_{ij} = \int_\Omega \phi_i \phi_j \, dx$,
- Stiffness matrix: $A_{ij} = \int_\Omega \nabla \phi_i \cdot \nabla \phi_j \, dx$,

The update formula becomes:

$$Mu^{n+1} = 2Mu^n - Mu^{n-1} - \Delta t^2 A u^n$$

2.4.4 Algorithm

At each time step n:

1. Compute the right-hand side:

$$\text{rhs} = 2Mu^n - Mu^{n-1} - \Delta t^2 A u^n$$

2. Solve:

$$Mu^{n+1} = \text{rhs}$$

3. Update:

$$u^{n-1} \leftarrow u^n, \quad u^n \leftarrow u^{n+1}$$

We are using an explicit scheme to solve a hyperbolic equation. This type of method requires a **CFL (Courant–Friedrichs–Lewy) stability condition**. For this 2D wave equation, the condition can be approximated by:

$$\boxed{\frac{dt}{h} \leq \frac{1}{\sqrt{2\pi}}}$$

For the sake of our simulation, we set dt **to** 0.002.

2.4.5 Spectral Decomposition Approach

An alternative method to solve this equation is to use apply what we studied previously.

Our previous study leads to targeting the following spectral problem:

$$-\Delta\phi_k = \lambda_k\phi_k \quad \text{in } \Omega, \qquad \phi_k|_{\partial\Omega} = 0,$$

where (λ_k, ϕ_k) are the eigenvalues and eigenfunctions of the Laplacian under Dirichlet boundary conditions.

We admit that the set $\{\phi_k\}_{k=1}^{\infty}$ forms an orthonormal basis of $L^2(\Omega)$ and also a complete basis in $H_0^1(\Omega)$.

We expand the solution $u(x, y, t)$ as:

$$u(x, y, t) = \sum_{k=1}^{\infty} \left(a_k \cos(\sqrt{\lambda_k}t) + b_k \sin(\sqrt{\lambda_k}t) \right) \phi_k(x, y),$$

where the coefficients a_k and b_k are determined by the initial conditions:

$$u(x, y, 0) = u_0(x, y) \quad \Rightarrow \quad a_k = \int_{\Omega} u_0(x, y)\phi_k(x, y)\, dx,$$

$$\left.\frac{\partial u}{\partial t}\right|_{t=0} = 0 \quad \Rightarrow \quad b_k = 0.$$

Thus, the solution reduces to:

$$u(x, y, t) = \sum_{k=1}^{\infty} a_k \cos(\sqrt{\lambda_k}t)\phi_k(x, y)$$

This approach is very efficient and accurate if we have access to a sufficiently large number of eigenmodes (λ_k, ϕ_k). It is especially useful for comparing against time-marching schemes, as it provides an "exact" semi-analytical benchmark for validation.

2.4.6 Comparison Between the Two Methods

To benchmark these two approaches, consider the scripts **NumericalResolution1.edp** and **NumericalResolution2.edp**. Both methods solve the wave equation on a square domain $\Omega = [0, 1] \times [0, 1]$, discretized using a uniform mesh of size 50×50. The initial condition is chosen as

$$u_0(x, y) = \sin(\pi x) \sin(\pi y)$$

which represents a smooth mode that satisfies homogeneous Dirichlet boundary conditions on all sides. The simulation time is set to $T = 2.0$ with a time step of $\Delta t = 0.01$, and the spectral method uses the first 500 eigenmodes to approximate the solution.

The spectral method, while highly accurate for problems with smooth solutions defined on simple domains, has notable drawbacks. It is often limited to regular geometries and simple boundary conditions, which restricts its applicability in more complex scenarios. Additionally, the spectral method can suffer from the Gibbs phenomenon near discontinuities, adversely affecting solution quality. In contrast, the finite element method (FEM) proves particularly effective for problems defined on complex geometries with varied boundary conditions. By adapting locally through mesh refinement and employing local shape functions, FEM offers great flexibility and maintains good accuracy even in the presence of singularities or discontinuities. Therefore, although spectral methods are advantageous in certain cases, the finite element method remains a robust and versatile choice for a wide range of scientific computing applications.

3 Graphene energy band computation

3.1

We consider the eigenvalue problem on the unit cell U, with periodic boundary conditions and a periodic potential V_{per}. For $V_{\text{per}} = 0$, the Bloch Hamiltonian is:

$$H_k u_k = \left(-\frac{1}{2}\Delta - ik \cdot \nabla + \frac{1}{2}|k|^2 \right) u_k = E_k u_k.$$

To obtain the variational formulation, we multiply the equation by the complex conjugate $\overline{v}$ of a test function $v \in H^1_{\text{per}}(U)$ and integrate over the unit cell U:

$$\int_U \left(\frac{1}{2}\nabla u_k \cdot \nabla \overline{v} + \frac{i}{2}(k \cdot \nabla u_k)\overline{v} - \frac{i}{2}u_k(k \cdot \nabla \overline{v}) + \frac{1}{2}|k|^2 u_k \overline{v} \right) dx = E_k \int_U u_k \overline{v}\, dx.$$

This is the variational formulation to implement in FreeFem++ using complex-valued finite element spaces.

3.2

3.2.a

You find the code of this question in the file `graphen_unitcell.edp`

3.2.b and 3.2.c and 3.2.d and 3.2.e

You find the code of these questions in the file `graphene_solver.edp` and the file `graphen_plot.py`